Translational structural and functional signatures of chronic alcohol effects in mice

Laëtitia Degiorgis, Tanzil Mahmud Arefin, Sami Ben-Hamida, Vincent Noblet, Cristina Antal, Thomas Bienert, Marco Reisert, Dominik von Elverfeldt, Brigitte Kieffer, Laura Harsan

Version of Record: https://www.sciencedirect.com/science/article/pii/S0006322322001007
Manuscript_380582707ef620d97c7209947a744d5a

Translational structural and functional signatures of chronic alcohol effects in mice

Short title: **Brain fingerprints of alcohol exposure**

Authors:

Laetitia Degiorgis[a*], Tanzil Mahmud Arefin[*b,c], Sami Ben-Hamida[d], Vincent Noblet[e], Cristina Antal[a,f], Thomas Bienert[b], Marco Reisert[b], Dominik von Elverfeldt[b], Brigitte L. Kieffer[d,g], and Laura-Adela Harsan[a,h*]

Affiliations:

[a] Laboratory of Engineering, Informatics and Imaging (ICube), Integrative multimodal imaging in healthcare team (IMIS), UMR 7357, University of Strasbourg, 4 Rue Kirschleger, 67000 Strasbourg, France

[b] Department of Radiology, Medical Physics, University Medical Center Freiburg, Faculty of Medicine, University Freiburg, 79085 Freiburg, Germany

[c] Bernanrd and Irene Schwartz Center for Biomedical Imaging, Department of Radiology, New York University Grossman School of Medicine, New York, NY 10016, USA

[d] Douglas Mental Health University Institute, Department of Psychiatry, McGill University Montreal, Canada

[e] Laboratory of Engineering, Informatics and Imaging (ICube), Images, Learning, Geometry and Statistics team (IMAGES), UMR 7357, University of Strasbourg, 4 Rue Kirschleger, 67000 Strasbourg, France

[f] Faculty of Medicine, University Hospital of Strasbourg, Histology Institute and Unité Fonctionnelle de Foetopathologie, 67000 Strasbourg,

[g] INSERM U1114, Dpt Psychiatry, University of Strasbourg, France

[h] Department of Biophysics and Nuclear Medicine, University Hospital of Strasbourg, 67000 Strasbourg, France

Key words: multimodal brain MRI, diffusion tensor imaging, resting state fMRI, functional connectivity, alcohol addiction, mouse models

***Corresponding author:** Laura-Adela Harsan: harsan@unistra.fr

ABSTRACT

BACKGROUND: Alcohol acts as an addictive substance which may lead to alcohol use disorder. In humans, Magnetic Resonance Imaging (MRI) showed diverse structural and functional brain alterations associated with this complex pathology. Single MRI modalities are mostly used, but are insufficient to portray and understand the broad neuroadaptations to alcohol. Here we combined structural and functional MRI and connectome mapping in mice, to establish brain wide fingerprints of alcohol effects with translatable potential.

METHODS: Mice underwent a chronic intermittent alcohol drinking protocol for six weeks before being imaged under medetomidine anaesthesia. We performed open-ended multi-variate analysis of structural data and functional connectivity mapping on the same subjects.

RESULTS: Structural analysis showed alcohol effects for prefrontal cortex/anterior insula (PFC/AI), hippocampus (HIP) and somatosensory cortex (SS). Integration with microglia histology revealed distinct alcohol signatures, suggestive of advanced (PFC/AI, SS) and early (HIP) inflammation. Functional analysis showed major alterations of AI, ventral tegmental area (VTA) and retrosplenial cortex (RSP) connectivity, impacting communication patterns for salience (AI), reward (VTA) and default mode (RSP) networks. AI appeared as a most sensitive brain center across structural and functional analyses.

CONCLUSIONS: This study demonstrates alcohol effects in mice, which possibly underlie lower top-down control and impaired hedonic balance documented at behavioral level, and aligns with neuroimaging findings in humans despite the potential limitation induced by medetomidine sedation. This study paves the way to identify further biomarkers, and to probe neurobiological mechanisms of alcohol effects using genetic and pharmacological manipulations in mouse models of alcohol drinking and dependence.

Abbreviations

ACA Anterior cingulate cortex

ACB Nucleus accumbens

AD Axial diffusivity

AI Agranular insula

ALC Volontary alcohol intake mice

AMG Amygdala nuclei

AUD Alcohol use disorder

BLA Basolateral amygdalar nucleus

BST Bed nuclei of the stria terminalis

cc Corpus callosum

CTRL Control

CEA Central amygdalar nucleus

CP Caudoputamen

(d)HIP (dorsal) hippocampus

DMN Default-mode network

DORpm Thalamus polymodal association cortex related

DTI Diffusion tensor imaging

ec External capsule

ECT Ectorhinal cortex

ENT Entorhinal cortex

FA Fractional anisotropy

FC Functional connectivity

FD Fiber density

fHIP Hipocampal formation

(rs)fMRI (resting state) functional Magnetic Resonance Imaging

GM Grey matter

HBN Habenula

MD Mean diffusivity

MO Motor cortex

MRI Magnetic Resonance Imaging

MRN Midbrain reticular nucleus

PERI Perirhinal cortex

PFC Prefrontal cortex

PIR Piriform cortex

RAmb Midbrain raphe nuclei

RD Radial diffusivity

RE Nucleus of reuniens

ROI Region of interest

RSP Retrosplenial cortex

SEP Septal nucleus

SS(p) (primary) Somatosensory

TH Thalamus

VTA Ventral tegmental area

WM White matter

Introduction

Alcohol use and abuse account for a tremendous burden of disease worldwide (1,2) and is a leading cause of physical and psychological harm to users and their social environment (3). After prolonged, repeated exposure, alcohol acts as an addictive substance that alters broad spectra of neuromolecular targets and signaling cascades (4), initiates genes expression changes, affects the synaptic function (5) and triggers functional and structural brain changes (6,7). Alcohol use disorder (AUD) is therefore considered a complex condition, characterized by distinct stages of the addiction cycle, associated to neuroadaptive brain changes (8).

In humans, Magnetic Resonance Imaging (MRI) studies extensively describe alcohol effects (9–12) highlighting vulnerability of the white matter (WM) (13–15) and revealing gray matter (GM) targets of alcohol use and abuse (16–18). Resting state functional MRI (rsfMRI) connectome investigations bring further evidence that chronic alcohol use leads to neurocircuitry adaptations across cognitive and emotional brain networks and across the alcoholism spectrum (19–23). Recent studies showed a link between patterns of functional connectivity (FC) and neuropathological conditions (24–27) in alcoholism.

Single MRI modalities are however insufficient to portray the complex AUD patterns. Multi-modal MRI and multi-parametric classifiers are necessary to better understand how structural abnormalities relate to alterations of brain function and how these imaging signatures capture, or even predict alcohol consumption behavior. Many of these factors are difficult to control and document in human investigations where mechanistic studies are challenging (28–31). Therefore, translation of these approaches in animal neuroimaging research is essential to reveal the neurobiological underpinnings of multivariate imaging signatures and to advance the quest of stratification markers of AUD.

In rodent behavioral models of alcohol exposure (32,33) longitudinal MRI studies have tracked the brain morphometric profiles (15,34–39) and Diffusion Tensor Imaging (DTI) revealed WM sensitivity to alcohol exposure (14). Limited information is available regarding the effects of alcohol on functional networks' architecture in rodents (20,40–45) and

multimodal studies combining structural and functional MRI are lacking in rodent models of alcohol drinking.

In the present study we carried out a multi-modal in-vivo MRI investigation to identify the consequences of alcohol consumption on brain wide structural and functional circuitries in a mouse model of voluntary drinking. We used the chronic two-bottle choice intermittent access paradigm (46,47), and developed advanced multivariate analysis of structural data (DTI, fiber tractography, morphometry, histopathology) and functional network mapping on the same subjects. Our analyses generate both structural and functional fingerprints of alcohol effects consistent with literature from alcoholism research in humans. This study also sets the basis for further whole brain neuroimaging investigations, using genetic and pharmacological manipulations in mouse models of alcohol drinking.

METHODS AND MATERIALS

Mice and alcohol exposure paradigm. Male mice (50% C57BL/6J - 50% 129Sv Pas) were used for all experiments (ethics 35_9185.81/G-13/15 from Freiburg-Germany and 2003-10-08-[1]-58, Strasbourg-France). Experimental details are given in Supplementary Information 1.1). Voluntary alcohol intake was tested using intermittent access two-bottle choice drinking alcohol paradigm (Fig.1, A) in mice (ALC; n=11), compared to a control group that had access to water only (CTRL; n=12) as previously described (40) and detailed in Supplementary Information 1.2.

In-vivo MRI experiments. 24h after the last alcohol drinking session, in-vivo mouse brain multimodal MRI was performed to acquire T2-weighed images, resting-state functional MRI (rsfMRI) and DTI data, as previously described (48). To evaluate significant structural differences between groups, we performed a multivariate analysis including parametric maps calculated from DTI and T2-weighted data. We generated spatial maps that combined all significant structural MRI parametric modifications in a global cluster. We then used a voxel-wise approach and assigned a specific structural signature of modifications for each voxel.

Voxels presenting similar pattern of multivariate structural modifications were extracted as clusters, covering specific brain regions. We further explored rsfMRI data to map FC using graph theory (49) and seed-based analysis. Detailed methods are provided in Supplementary Information 1.3.

Immunohistological staining. To investigate the brain microstructural substrate of alcohol-induced modifications, we performed IBA1 and GFAP immunostaining of microglia and astrocytes, as described in Supplementary Information 1.4.

RESULTS

Setting up alcohol drinking for MRI investigations

We used a classical model of voluntary alcohol drinking - the intermittent two-bottle choice drinking procedure (Figure 1A) - known to lead to high levels of alcohol consumption in mice (40). Levels of alcohol drinking stabilized over the sessions (Figure 1B) and the mean alcohol intake during the whole experiment was of 11.06 g/kg body weight / 24 hours (one-sample t-test, $p<0.05$). Water intake was comparable in the two ALC and CTRL groups. Image acquisition was performed 24 hours after the last alcohol drinking session, leaving animals in a withdrawal/abstinent state.

Open-ended structural MRI reveals distinct alcohol signatures in PFC/AI, HIP and SS

To investigate potential structural modifications in ALC mice, we conducted a data-driven multivariate analysis combining DTI-derived quantitative parametric indices and voxel-based morphometry results (Figure 2A-D). Overall results are mapped in Figure 2A and E, indicating brain areas significantly impacted by alcohol in GM and WM respectively. We identified three GM clusters (Figures 2B, C, D) and one WM cluster (Figure 2F), each characterized by a specific structural MRI multi-parametric signature.

For the GM regions, a first cluster, covering the prefrontal cortex (PFC) and partially the insular cortex (AI), featured significantly higher diffusivity values in ALC mice compared to CTRL (Figure 2B) including axial (AD, $z = 2.98$), radial (RD, $z = 2.61$) and mean (MD, $z =$

2.76) diffusivity. The fractional anisotropy (FA), depending on RD and AD values, was also higher in the PFC/AI (z = 2.57), a likely consequence of the high AD increase in ALC mice. Morphometry measurements showed a volumetric decrease of these areas (logjacobian, z = -2.13), while fibers density (FD) mapping derived from tractography showed higher values (FD, z = 2.66). Forming a second cluster, dorsal hippocampus (dHIP) presented a very different pattern of structural modifications (Figure 2C). FA values were significantly higher (z = 2.84) in the ALC group compared to CTRL, whereas decreased diffusivity values were found for AD (z = -2.1), RD (z = -2.98), and MD (z = -2.83). A third pattern of structural MRI signatures covered the somatosensory (SS) cortex of ALC mice (Figure 2D), showing a tendency for lower diffusivity values for MD (z = -1.85), RD (z = -1.83) and AD (z = -1.71). Morphometric measurements detected a significant decrease of SS volume (z = -2.09.16) in ALC mice (Figure 2D). Finally, a WM cluster (Figure 2E) covering the corpus callosum (cc) and the external capsule (ec) showed a similar pattern of change in ALC mice as for the dHIP, characterized by higher FA values (z = 3.49) and lower diffusivity in RD (z = -2.3), MD (z = -2.2) and AD (z = -1.79).

In sum, our analysis detected significant effects of voluntary alcohol drinking on the mouse brain microstructure, with distinct multivariate signatures characterizing PFC/AI, dHIP, SS and cc/ec areas.

Alcohol exposure induces activation of microglia and astrocytes in PFC/AI and HIP

To investigate the neurobiological basis for microstructural differences induced by alcohol drinking, we examined neuroinflammatory processes considered essential in alcohol-related neuroadaptations (50). We focused on AI, PFC and HIP (Figure 3), the main nodes for plasticity identified in our functional and structural MRI analysis. We performed IBA1 and GFAP immunostaining of microglia and astrocytes. We quantitatively evaluated the surface (% area) of marked cells (for both IBA1 and GFAP), as well as the number of microglial cells (for IBA1). GFAP % area quantification revealed an astrogliosis trend in PFC/AI (p=0.0525) and HIP (p=0.047, data not shown), associated with cell reshaping into dominant bipolar

features in the ALC group, specific to astrocytic activation. IBA1 staining revealed comparable changes in the PFC and AI of ALC mice, characterized by significant increase in microglial cell number for ALC mice with higher statistical significance for PFC (Figures 3A). This was associated with microglial shape changes: less ramified cell processes with larger extra-cellular space for ALC mice (Figure 3B) resulted in a lower % of IBA1 stained surface compared with the CTRL brains in AI and PFC. A different pattern was observed in HIP (Figure 3A), which also showed significant increase of microglial cells ($p<0.001$), but combined with increased IBA1 staining coverage for ALC mice. Altogether therefore, alcohol increased the number of microglial cells in all three regions, accompanied with either cell processes shrinking (AI, PFC) or hypertrophy (HIP), consistent with the distinct MRI signatures.

We next integrated structural multi-parametric MRI (Figure 2) and histological quantification of microglial activity (Figure 3B) to provide a fingerprint of structural modifications in the PFC/AI and HIP of alcohol-exposed mice. In the PFC/AI areas (Figure 3C), the global significant increase of DTI-derived features was associated with microglial activation and processes shrinking, suggestive of inflammatory processes that may have led to other tissue damages. In contrast, the HIP signature (Figure 3D) showed a significant increase of FA only, associated with increased number of activated, ramified microglial cells, a likely hallmark of an earlier phase of neuro-inflammation.

Graph network analysis of rs-fMRI data demonstrates major alteration of AI, VTA and RSP connectivity

We further evaluated FC differences using graph network analysis. We focused on a circuit of 26 brain regions known for their involvement in drug reward, alcohol seeking and drinking behavior (5,6). We first used the 26x26 FC matrix to characterize group-specific FC patterns (Figure 4), and mapped the FC organization of statistically significant connected nodes for each group (network diagrams, Figures 4A and B). We ranked these nodes according to their significance in “degree”, and also show their associated significant “hubness” (Figures 4A

and B – graph bars). Overall, there was a lower number of significantly connected nodes in ALC (20) compared to CTRL (23) mice. The most significant node in terms of degree was the HIP for both groups. However, in ALC mice, graph network diagrams highlighted hyper-connectivity of RSP, appearing as the second most influential node in the ALC brains for the number of significant connections (degree=7), and showing highest hubness values (10.3). Further, reward-related nodes decreased their hubness, including the ACB (ALC 3.3 vs CTRL 4.6), VTA and RAmb (not-significant in ALC group). In contrast, aversion-related nodes strengthened their importance as hubs in ALC mice, including habenula (HBN, ALC 5.7 vs. CTRL 4.6) and central amygdala (CEA, ALC 1.1 vs CTRL non-significant), suggesting altogether modifications in the hedonic balance.

Next, we carried-out an inter-group statistical comparison of FC matrices (ACL vs. CTRL; two-sample t-test, $p<0.05$, uncorr.), showing alcohol sensitive nodes and connections (Figure 4C and D). We established a ranking for most changed nodes (Stouffer coefficient, $p<0.05$, uncorr., Figure 4C), and summarized significantly changed connections graphically (Figure 4D). We found significant FC differences for three nodes: AI, VTA and RSP. As regards to their connectivity, edges connecting AI to DORpm ($p=0.0009$), prefrontal cortex (PFC; $p=0.022$), raphe nuclei ($p=0.034$), hippocampal formation (PERI/ECT/ENT or fHIP; $p=0.038$) and the septum (SEP; $p=0.048$) were significantly modified in ALC compared to CTRL mice. Additionally, core nodes of the Default Mode Network (DMN), the RSP and ACA, showed strongly modified connectivity with sensory areas in the ALC group: RSP with olfactory cortical areas (RSP - PIR connection; $p=0.037$) and ACA with somatosensory cortex (ACA – SSp connection; $p=0.001$). FC was also modified for VTA – ACA ($p=0.010$), representative for DMN-reward inter-network connectivity. Finally, some other significant FC alterations were observed, involving basal ganglia/extended amygdala nodes and connections (SEP, CP, CEA, BLA) (Figure 4C).

In conclusion, three brain areas and their associated connections show most significant differences: the AI – hub of the salience network; VTA – core node of the

mesocorticolimbic dopamine circuitry and key for reward/aversion mechanisms; RSP –main driver of the DMN in the rodent brain.

Seed voxel-wise analysis of rsfMRI data reveals alcohol FC patterns for salience (AI), reward (VTA) and default mode network (RSP) nodes

To acquire a brain-wide view of functional alterations for the three major alcohol-modified nodes, we performed a seed-based voxel-wise inter-group comparison ($p<0.05$, FDR cluster-corrected; Figure 5). We examined FC for AI (salience), VTA (reward) and RSP (DMN), and also explored the PFC, amygdala (AMG), bed nuclei of stria terminalis (BST) and SS (Suppl. Figure 2) networks, as they showed either strong modifications in our structural analysis, or have been largely associated with alcohol seeking/drinking behavior (19,21,40,45,51). First, AI significantly increased its connectivity with somatomotor cortices (SS and MO) and VTA following ALC exposure (Figure 5A). Next, alcohol consumption induced VTA hyperconnectivity with core regions of reward (ACB, CP), aversion (HBN), salience (AI) and DMN (ACA and RSP) (Figure 5B). VTA additionally showed increased FC with nucleus of reuniens (RE), thalamic area associated with memory processes. Third, alcohol drinking altered RSP's FC (Figure 5C), with increased patterns toward somatomotor cortices, substantia nigra (SN), midbrain reticular nucleus (MRN) and thalamic areas (TH). Finally, modifications of PFC FC (Suppl Figure 2) included significantly weaker PFC - AI connectivity in ALC compared to the CTRL mice, but stronger FC between PFC and CP, AMG and VTA

Data from seed-based analysis (Figure 5A, B, C and Suppl. Figure 2) are summarized in network diagram (Figure 5D), representing significant voxel-wise FC modifications, with a focus on AI, VTA and RSP. In sum, this analysis shows strong alterations of salience (AI), reward (VTA) and DMN (RSP) -like networks, with basal ganglia (ACB, BST, CP) and aversive subcortical centers (AMG, HBN) and several cortical areas (PFC, HIP, SS).

DISCUSSION

In this study, we used the 2-bottle choice chronic intermittent access paradigm (40,47,52–54), considered a standard model of excessive voluntary alcohol drinking in mice. We performed non-invasive MRI in these mice and analyzed their brain state after 6 weeks drinking using multi-parametric structural MRI and classification approaches, as well as mapping of intrinsic functional networks' architecture. Our data provide in-vivo fingerprints of alcohol-induced modifications of both microstructural and functional connectome, capturing brain-wide and regional effects of chronic alcohol consumption.

Structural MRI indicators point to specific modifications in GM areas, shown critical in human AUD (6,16,51,55), including prefrontal, insular and sensory-motor cortices and hippocampus. We mapped region-specific microstructural patterns – possibly accounting for differential vulnerability or reactivity to alcohol, or highlighting time-dependent evolution of the pathology. The results were attuned with ex-vivo findings of differential histopathologic patterns of microglial and inflammatory processes.

We further show in the same animals, perturbed functional inter-play between driver-nodes of salience (AI), reward (VTA) and default mode networks (RSP). FC modifications include basal ganglia (ACB, BST, CP and AMG), aversive subcortical centers (HBN) and executive as well as sensory control areas (PFC, SS), all evocative of connectome modifications described in AUD (19,56). The key findings are schematically summarized in Figure 6, showing areas found most affected from structural analysis and FC alterations. It is of note that, in our multimodal analysis, PFC/AI is a key disrupted brain region at both structural and functional levels.

The analysis of microstructural modifications uncovers region-specific fingerprints

Multivariate statistics of structural MRI identified three different parametric profiles of significant alcohol effects in GM, spatially localized in PFC/AI, SS, and HIP. This data-driven finding is consistent with previous reports of altered cortical and subcortical systems involving the PFC, HIP and SS (57) in both human and rodents (58–62) .

The first cluster – overlapping PFC and partly AI shows increase of all diffusivity values, with higher increase of AD - associated to main diffusion/fibers orientation - than RD and resulting in a significant FA elevation. This particular parametric signature relates to immunohistochemistry findings in PFC/AI, showing a greater number of microglial cells but reduced/depleted ramifications in ALC mice. This is suggestive of an activated microglial phenotype, often described in the context of ongoing neurodegeneration and neurotoxicity (63). Therefore, higher diffusivity indices in PFC/AI might reflect combined inflammatory and degenerative processes, enlargement of extracellular space and/or cellular loss. Alcohol consumption has indeed been related to neuroinflammation (50,64,65) and neurodegeneration in postmortem human alcoholics (66) and mice treated with ethanol (64,67).

The second (HIP) and *the third (SS) clusters* of significant alcohol induced effects identified by multivariate classification as well as the WM cluster (cc/ec); are characterized by lower diffusivity and higher FA. The higher density of IBA1+ cells with highly ramified profile in the HIP of ALC mice correspond to an earlier stage of microglial reactivity and proliferation (68), although other microstructural affectations cannot be excluded. Reduced AD and RD values were previously associated with early phase of microglial, astrocytes infiltration, and acute axonal damage in mice (69,70). However, these reduced diffusivities could also reflect the development of cytotoxic brain edema (71).

While interpretation of some diffusion parameters can be challenging (72), they have been extensively used to better understand the physiopathology of brain diseases (73–76) investigating combined white and grey matter changes (77–83).

Modifications in diffusion parameters have been associated to different stages of Wallerian degeneration in axons, initiating an inflammatory response (84). According to the profile of diffusion indices, microstructural alterations following a nerve injury could be divided in two phases: (i) decrease of diffusion parameters would be related to the earliest stage of neuroinflammation (microglial proliferation) whereas (ii) gradual increase of MD, AD, RD have been associated with the later phase of neuropathological processes, including

microglial activation with morphology changes; myelin clearance and astrocytosis (84). A recent translational study in chronically drinking humans and rats associated a widespread increased MD in the brain GM with robust decrease in extracellular space tortuosity explained by reduction of microglia complexity (85). Additionally, ethanol abstinent rats (86) showed increased MD occurring concomitantly with increases in myelin associated proteins, flayed myelin, enhanced mitochondrial stress and neuroinflamatory response in medial PFC. In coherence with our histological findings, we therefore suggest that the observed microstructural modifications in the PFC, HIP and SS could be related to differential stages of the neuroinflammatory and neurodegenerative process. In PFC, the global increase of diffusion parameters, might reflect more advanced pathology associated with alcohol induced neurotoxicity and characterized by reactive microglia, astrogliosis and possibly ongoing axonal and myelin damage (50,64,66,67).

In our study we also report regional morphometric divergence in the ALC mice: (i) decreased volume of the PFC/AI and SS, where advanced inflammatory processes might lead to various degenerative processes; (ii) enlarged HIP volume corroborating a different pattern of IBA1 staining. Similarly, a group exploring a transgenic mouse presenting higher alcohol consumption detected decreased volume of the PFC and SS but not HIP (87). Alcohol related brain volume changes have been previously reported in human (55,88) studies, showing reduction in fronto-parietal areas including PFC, AI, and brain reward system as well as white matter tracts (89), also consistent with our functional analysis.

Finally, higher FA values were intriguingly but constantly observed in our study and positively correlated with alcohol consumption (Suppl Figure1). McEvoy et al., recently examined the WM FA as a function of alcohol intake in Human, and found increased FA in several major tracts – including cc - with increasing alcohol intake, reaching a maximum at the moderate drinking level, and only decreasing with greater alcohol intake. Because many studies previously reported decreased FA values related to AUD mechanisms or abstinence (9,10,58,86), we suggest that our findings might capture ongoing moderate pathology.

Impaired inter-networks communication reflects corticolimbic dysfunction.

Our functional analysis identified remodeling of network connectivity. We show with graph theory a strong impact of alcohol drinking on hubness properties of cortical FC nodes, notably RSP and SS. In addition, reward/aversion centers of the mesocorticolimbic circuitry (VTA, ACB and HBN) as well as basal ganglia (CP, SEP, PAL, BST and CEA) showed altered (decreased or increased) hubness, suggestive of unbalanced processing of the reward/aversion mechanisms at circuitry level. Direct statistical comparison of FC matrices of ALC and CTRL groups completed the picture with alterations of AI and the salience network, and seed-based analysis revealed modified communication between AI and reward/aversion and default mode systems. The latter analysis also highlighted FC differences of other nodes, which were also identified in the multivariate structural analysis: (i) the PFC/ACA - involved in decision-making and inhibitory control behavior in alcohol dependency (51); (ii) SS/MO areas, (iii) HIP network and (iv) basal ganglia nodes (ACB, BNT, AMG). This overlap between structural and functional findings is in line with the structural-functional correspondence hypothesis of brain networks (90,91).

Our findings from the rsfMRI analysis are aligned with both preclinical and human studies - consistently showing perturbed mesocorticolimbic communication in AUD (19,92). In rodent research, VTA has been widely described as crucial node of this system, regulating dopamine release in addiction and responsible for the craving state in alcohol dependency (44,93,94). Our results indicate increased FC of the VTA with other reward centers including ACA, ACB, CP, HBN, HIP; and the thalamus. Several pathological mechanisms have been associated with an increased inter-network FC and hyperconnectivity (95–97), which could be explained as a maladaptive mechanism mediated by dedifferentiation of functional networks (98). Other studies in mice showed a predictive link between elevated activity within reward-related networks and vulnerability for alcoholism (51,99). A comparable intermittent ethanol exposure protocol in mice (93) generated similar hyperexcitability of the cortico-striatal pathway. The hypersynchrony of the VTA's rsfMRI signal with other reward areas (notably ACB) might be related to increased firing rate of dopamine neurons led by chronic

alcohol consumption (94,100) and/or an increase of its release in the ACB (101). In humans, VTA-RSP and VTA-ACA increased inter-communication – as seen in the seed-based analysis - has been associated with increased anxiety in alcoholics (23). RSP and ACA nodes are central for the DMN state, and DMN changes in AUD have been largely associated to disrupted cognitive and emotional functions. DMN disrupted interaction with other networks, including salience and the executive control network (102) is known to affect cognition, emotion, attention and impulsivity, contributing to craving and relapse in substance use disorders (23). Moreover, the weakened "willpower" of alcohol users has been suggested to be the consequence of the disruption of a triadic model (56) involving the AI, PFC, and basal ganglia networks.

RsfMRI acquisition in our study was performed under anesthesia using the alpha-2-adrenergic agonist medetomidine. Based in literature (103–106), medetomidine at low doses induces sedation rather than full anesthesia, and reasonably preserves the integrity of FC networks as compared to awake rodents. Nevertheless, we cannot exclude a specific impact of the medetomidine sedation on the FC of ethanol exposed mice. Repeated dexmedetomidine subcutaneous administration during withdrawal was previously reported to lead to a decrease of withdrawal symptoms in rats exposed to alcohol (107). So far no data are available regarding such an interaction and its impact on the functional connectome.

Of note is that AI was identified from both structural and functional analyses as a brain center strongly altered by alcohol exposure (Figure 6). Similar changes were found in AUD patients (108) using graph-based analysis, showing stronger connectivity and increased centrality of the anterior insula associated with increased risk of relapse. AI may therefore drive integration of interoceptive states in AUD, coherently with AI within-networks FC modifications that have been associated with motivation and alcohol craving (19). Consistently, several preclinical studies showed that functional modulation of insula (93,109) significantly alters alcohol intake. This brain structure mediates interoceptive effects of alcohol (110) and addiction-related internal states (112,114). Particularly, the anterior insula presenting a distinct connectivity pattern from posterior/medial insula (111), would drive

alcohol consumption despite negative consequences (113,115). All these roles may modulate the alcohol intake (116), therefore AI structure and function may represent both a biomarker and a mechanistic basis to evaluate and understand AUD.

Conclusions

With multimodal structural and functional MRI performed in the same subjects, we here identify several signatures of alcohol-induced neuroadaptations in mice, pointing at strong and possibly early sensitivity of the PFC/AI. More broadly, the preclinical model of excessive alcohol drinking used in this study identifies brain-wide alterations, possibly underlying the lower top-down control and impaired hedonic balance typically observed at behavioral level (117). Finally, our data also corroborate neuroimaging results in humans (19,56), paving the way to identify further translatable biomarkers and probe circuit and/or treatment mechanisms using genetic and pharmacological manipulations in mouse models of alcohol drinking and addiction.

ACKNOWLEDGEMENTS AND DISCLOSURES

This work was supported by the National Institute of Health (National Institute on Alcohol Abuse and Alcoholism, Grant No. 16658, BK). The authors acknowledge the funding grants from Brain Links Brain Tools (BLBT) cluster of excellence from Freiburg (MouseNet 31 project). This project was funded with support from the NeuroTime Erasmus+: Erasmus Mundus program of the European Commission. This publication/communication reflects the views only of the author, and the Commission cannot be held responsible for any use that may be made of the information contained therein. The authors acknowledge the in-vivo imaging platform of ICube Lab - IRIS, Strasbourg, France for the participation to MRI data analysis, and particularly Mary Mondino. The authors also acknowledge Dr. Julien Lamy for his help and guidance related to image processing methodology. All authors critically reviewed the content and approved the final version before submission. All data needed to

evaluate the conclusions in the article are present in the article and/or supplementary material. Additional data related to this article are available upon request from the corresponding author. The authors report no biomedical financial interests or potential conflicts of interest.

REFERENCES

1. Grant BF, Goldstein RB, Saha TD, Chou SP, Jung J, Zhang H, *et al.* (2015): Epidemiology of DSM-5 Alcohol Use Disorder: Results From the National Epidemiologic Survey on Alcohol and Related Conditions III. *JAMA Psychiatry* 72: 757–766.
2. Rehm J, Shield KD, Gmel G, Rehm MX, Frick U (2013): Modeling the impact of alcohol dependence on mortality burden and the effect of available treatment interventions in the European Union. *Eur Neuropsychopharmacol J Eur Coll Neuropsychopharmacol* 23: 89–97.
3. Nutt DJ, King LA, Phillips LD, Independent Scientific Committee on Drugs (2010): Drug harms in the UK: a multicriteria decision analysis. *Lancet Lond Engl* 376: 1558–1565.
4. Ron D, Barak S (2016): Molecular mechanisms underlying alcohol-drinking behaviours. *Nat Rev Neurosci* 17: 576–591.
5. Roberto M, Varodayan F (2017): Synaptic Targets: Chronic Alcohol Actions. *Neuropharmacology* 122: 85–99.
6. Geibprasert S, Gallucci M, Krings T (2010): Alcohol-induced changes in the brain as assessed by MRI and CT. *Eur Radiol* 20: 1492–1501.
7. Fede SJ, Grodin EN, Dean SF, Diazgranados N, Momenan R (2019): Resting state connectivity best predicts alcohol use severity in moderate to heavy alcohol users. *NeuroImage Clin* 22: 101782.
8. Pandey SC, Kyzar EJ, Zhang H (2017): Epigenetic basis of the dark side of alcohol addiction. *Neuropharmacology* 122: 74–84.
9. Pfefferbaum A, Rosenbloom M, Rohlfing T, Sullivan EV (2009): Degradation of Association and Projection White Matter Systems in Alcoholism Detected with Quantitative Fiber Tracking. *Biol Psychiatry* 65: 680–690.
10. Yeh P-H, Simpson K, Durazzo TC, Gazdzinski S, Meyerhoff DJ (2009): Tract-based spatial statistics (TBSS) of diffusion tensor imaging data in alcohol dependence: Abnormalities of the motivational neurocircuitry. *Psychiatry Res Neuroimaging* 173: 22–30.
11. Dupuy M, Chanraud S (2016): Imaging the Addicted Brain: Alcohol. *Int Rev Neurobiol* 129: 1–31.
12. Tsurugizawa T, Abe Y, Le Bihan D (2017): Water apparent diffusion coefficient correlates with gamma oscillation of local field potentials in the rat brain nucleus accumbens following alcohol injection. *J Cereb Blood Flow Metab* 37: 3193–3202.
13. Pfefferbaum A, Sullivan EV (2002): Microstructural but not macrostructural disruption of white matter in women with chronic alcoholism. *NeuroImage* 15: 708–718.
14. Pfefferbaum A, Zahr NM, Mayer D, Rohlfing T, Sullivan EV (2015): Dynamic Responses of Selective Brain White Matter Fiber Tracts to Binge Alcohol and Recovery in the Rat. *PLoS ONE* 10. https://doi.org/10.1371/journal.pone.0124885
15. Zahr NM, Pfefferbaum A (2017): Alcohol's Effects on the Brain: Neuroimaging Results in Humans and Animal Models. *Alcohol Res Curr Rev* 38: 183–206.
16. Mechtcheriakov S, Brenneis C, Egger K, Koppelstaetter F, Schocke M, Marksteiner J (2007): A widespread distinct pattern of cerebral atrophy in patients with alcohol addiction revealed by voxel-based morphometry. *J Neurol Neurosurg Psychiatry* 78: 610–614.
17. Wilhelm J, Frieling H, Hillemacher T, Degner D, Kornhuber J, Bleich S (2008): Hippocampal volume loss in patients with alcoholism is influenced by the consumed type of alcoholic beverage. *Alcohol Alcohol Oxf Oxfs* 43: 296–299.
18. Durazzo TC, Tosun D, Buckley S, Gazdzinski S, Mon A, Fryer SL, Meyerhoff DJ (2011): Cortical Thickness, Surface Area and Volume of the Brain Reward System in Alcohol Dependence: Relationships to Relapse and Extended Abstinence. *Alcohol Clin Exp Res* 35: 1187–1200.
19. Zhu X, Cortes CR, Mathur K, Tomasi D, Momenan R (2017): Model-free functional connectivity and impulsivity correlates of alcohol dependence: a resting-state study. *Addict Biol* 22: 206–217.

20. Broadwater MA, Lee S-H, Yu Y, Zhu H, Crews FT, Robinson DL, Shih Y-YI (2018): Adolescent alcohol exposure decreases frontostriatal resting-state functional connectivity in adulthood. *Addict Biol* 23: 810–823.
21. Hu S, Ide JS, Chao HH, Zhornitsky S, Fischer KA, Wang W, *et al.* (2018): Resting state functional connectivity of the amygdala and problem drinking in non-dependent alcohol drinkers. *Drug Alcohol Depend* 185: 173–180.
22. Zhornitsky S, Ide JS, Wang W, Chao HH, Zhang S, Hu S, *et al.* (2018): Problem Drinking, Alcohol Expectancy, and Thalamic Resting-State Functional Connectivity in Nondependent Adult Drinkers. *Brain Connect* 8: 487–502.
23. Zhang R, Volkow ND (2019): Brain default-mode network dysfunction in addiction. *NeuroImage* 200: 313–331.
24. Huang Y, Mohan A, De Ridder D, Sunaert S, Vanneste S (2018): The neural correlates of the unified percept of alcohol-related craving: a fMRI and EEG study. *Sci Rep* 8: 923.
25. Gerchen MF, Weiss F, Kirsch M, Rentsch A, Halli P, Kiefer F, Kirsch P (n.d.): Dynamic frontostriatal functional peak connectivity (in alcohol use disorder). *Hum Brain Mapp* n/a. https://doi.org/10.1002/hbm.25201
26. Stein M, Steiner L, Fey W, Conring F, Rieger K, Andrea F, Moggi F (2020): Alcohol-related context modulates neural correlates of inhibitory control in alcohol dependent patients: preliminary data from an fMRI study using an alcohol-related Go/NoGo-task. *Behav Brain Res* 112973.
27. Burnette EM, Grodin EN, Ghahremani DG, Galván A, Kohno M, Ray LA, London ED (2020): Diminished cortical response to risk and loss during risky decision making in alcohol use disorder. *Drug Alcohol Depend* 108391.
28. Porjesz B, Rangaswamy M, Kamarajan C, Jones KA, Padmanabhapillai A, Begleiter H (2005): The utility of neurophysiological markers in the study of alcoholism. *Clin Neurophysiol Off J Int Fed Clin Neurophysiol* 116: 993–1018.
29. Fein G, Landman B (2005): Treated and treatment-naive alcoholics come from different populations. *Alcohol Fayettev N* 35: 19–26.
30. Pfefferbaum A, Sullivan EV, Mathalon DH, Shear PK, Rosenbloom MJ, Lim KO (1995): Longitudinal changes in magnetic resonance imaging brain volumes in abstinent and relapsed alcoholics. *Alcohol Clin Exp Res* 19: 1177–1191.
31. Becker HC (2000): Animal Models of Alcohol Withdrawal. *Alcohol Res Health* 24: 105–113.
32. Spanagel R (2003): Alcohol addiction research: from animal models to clinics. *Best Pract Res Clin Gastroenterol* 17: 507–518.
33. Zahr NM, Sullivan EV (2008): Translational studies of alcoholism: bridging the gap. *Alcohol Res Health J Natl Inst Alcohol Abuse Alcohol* 31: 215–230.
34. Fritz M, Klawonn AM, Zahr NM (2019): Neuroimaging in Alcohol Use Disorder: from mouse to man. *J Neurosci Res*. https://doi.org/10.1002/jnr.24423
35. Sullivan EV, Adalsteinsson E, Sood R, Mayer D, Bell R, McBride W, *et al.* (2006): Longitudinal brain magnetic resonance imaging study of the alcohol-preferring rat. Part I: adult brain growth. *Alcohol Clin Exp Res* 30: 1234–1247.
36. Zahr NM, Lenart AM, Karpf JA, Casey KM, Pohl KM, Sullivan EV, Pfefferbaum A (2020): Multi-modal imaging reveals differential brain volumetric, biochemical, and white matter fiber responsivity to repeated intermittent ethanol vapor exposure in male and female rats. *Neuropharmacology* 170: 108066.
37. Gass N, Cleppien D, Zheng L, Schwarz AJ, Meyer-Lindenberg A, Vollmayr B, *et al.* (2014): Functionally altered neurocircuits in a rat model of treatment-resistant depression show prominent role of the habenula. *Eur Neuropsychopharmacol J Eur Coll Neuropsychopharmacol* 24: 381–390.
38. Gozzi A, Agosta F, Massi M, Ciccocioppo R, Bifone A (2013): Reduced limbic metabolism and fronto-cortical volume in rats vulnerable to alcohol addiction. *NeuroImage* 69: 112–119.

39. Fish EW, Holloway HT, Rumple A, Baker LK, Wieczorek LA, Moy SS, *et al.* (2016): Acute alcohol exposure during neurulation: Behavioral and brain structural consequences in adolescent C57BL/6J mice. *Behav Brain Res* 311: 70–80.
40. Ben Hamida S, Mendonça-Netto S, Arefin TM, Nasseef MT, Boulos L-J, McNicholas M, *et al.* (2018): Increased Alcohol Seeking in Mice Lacking Gpr88 Involves Dysfunctional Mesocorticolimbic Networks. *Biol Psychiatry* 84: 202–212.
41. Dudek M, Hyytiä P (2016): Alcohol preference and consumption are controlled by the caudal linear nucleus in alcohol-preferring rats. *Eur J Neurosci* 43: 1440–1448.
42. Dudek M, Canals S, Sommer WH, Hyytiä P (2016): Modulation of nucleus accumbens connectivity by alcohol drinking and naltrexone in alcohol-preferring rats: A manganese-enhanced magnetic resonance imaging study. *Eur Neuropsychopharmacol J Eur Coll Neuropsychopharmacol* 26: 445–455.
43. Rodriguez CI, Davies S, Calhoun V, Savage DD, Hamilton DA (2016): Moderate Prenatal Alcohol Exposure Alters Functional Connectivity in the Adult Rat Brain. *Alcohol Clin Exp Res* 40: 2134–2146.
44. Hadar R, Vengeliene V, Barroeta Hlusicke E, Canals S, Noori HR, Wieske F, *et al.* (2016): Paradoxical augmented relapse in alcohol-dependent rats during deep-brain stimulation in the nucleus accumbens. *Transl Psychiatry* 6: e840.
45. Perez-Ramirez U, Diaz-Parra A, Ciccocioppo R, Canals S, Moratal D (2017): Brain functional connectivity alterations in a rat model of excessive alcohol drinking: A resting-state network analysis. *Annu Int Conf IEEE Eng Med Biol Soc IEEE Eng Med Biol Soc Annu Int Conf* 2017: 3016–3019.
46. Wise RA (1973): Voluntary ethanol intake in rats following exposure to ethanol on various schedules. *Psychopharmacologia* 29: 203–210.
47. Melendez RI (2011): Intermittent (every-other-day) drinking induces rapid escalation of ethanol intake and preference in adolescent and adult C57BL/6J mice. *Alcohol Clin Exp Res* 35: 652–658.
48. Arefin TM, Mechling AE, Meirsman AC, Bienert T, Hübner NS, Lee H-L, *et al.* (2017): Remodeling of Sensorimotor Brain Connectivity in *Gpr88* -Deficient Mice. *Brain Connect* 7: 526–540.
49. Sporns O (2018): Graph theory methods: applications in brain networks. *Dialogues Clin Neurosci* 20: 111–121.
50. Erickson EK, Grantham EK, Warden AS, Harris RA (2019): Neuroimmune signaling in alcohol use disorder. *Pharmacol Biochem Behav* 177: 34–60.
51. Alasmari F, Goodwani S, McCullumsmith RE, Sari Y (2018): Role of glutamatergic system and mesocorticolimbic circuits in alcohol dependence. *Prog Neurobiol* 171: 32–49.
52. Carnicella S, Ron D, Barak S (2014): Intermittent ethanol access schedule in rats as a preclinical model of alcohol abuse. *Alcohol Fayettev N* 48: 243–252.
53. Hwa LS, Chu A, Levinson SA, Kayyali TM, DeBold JF, Miczek KA (2011): Persistent escalation of alcohol drinking in C57BL/6J mice with intermittent access to 20% ethanol. *Alcohol Clin Exp Res* 35: 1938–1947.
54. Rosenwasser AM, Fixaris MC, Crabbe JC, Brooks PC, Ascheid S (2013): Escalation of intake under intermittent ethanol access in diverse mouse genotypes. *Addict Biol* 18: 496–507.
55. Makris N, Oscar-Berman M, Jaffin SK, Hodge SM, Kennedy DN, Caviness VS, *et al.* (2008): Decreased volume of the brain reward system in alcoholism. *Biol Psychiatry* 64: 192–202.
56. Noël X, Brevers D, Bechara A (2013): A Triadic Neurocognitive Approach to Addiction for Clinical Interventions. *Front Psychiatry* 4: 179.
57. Aransay A, Rodríguez-López C, García-Amado M, Clascá F, Prensa L (2015): Long-range projection neurons of the mouse ventral tegmental area: a single-cell axon tracing analysis. *Front Neuroanat* 9. https://doi.org/10.3389/fnana.2015.00059
58. De Santis S, Bach P, Pérez-Cervera L, Cosa-Linan A, Weil G, Vollstädt-Klein S, *et al.* (2019): Microstructural White Matter Alterations in Men With Alcohol Use Disorder

and Rats With Excessive Alcohol Consumption During Early Abstinence. *JAMA Psychiatry* 76: 749–758.
59. Gao L, Grebogi C, Lai Y-C, Stephen J, Zhang T, Li Y, *et al.* (2019): Quantitative assessment of cerebral connectivity deficiency and cognitive impairment in children with prenatal alcohol exposure. *Chaos Woodbury N* 29: 041101.
60. Oladehin A, Margret CP, Maier SE, Li CX, Jan TA, Chappell TD, Waters RS (2007): Early Postnatal Alcohol Exposure Reduced the Size of Vibrissal Barrel Field in Rat Somatosensory Cortex (SI) but Did Not Disrupt Barrel Field Organization. *Alcohol Fayettev N* 41: 253–261.
61. Margret CP, Li CX, Chappell TD, Elberger AJ, Matta SG, Waters RS (2006): Prenatal alcohol exposure delays the development of the cortical barrel field in neonatal rats. *Exp Brain Res* 172: 1–13.
62. O'Herron P, Summers PM, Shih AY, Kara P, Woodward JJ (2020): In vivo two-photon imaging of neuronal and brain vascular responses in mice chronically exposed to ethanol. *Alcohol Fayettev N* 85: 41–47.
63. Burguillos MA, Deierborg T, Kavanagh E, Persson A, Hajji N, Garcia-Quintanilla A, *et al.* (2011): Caspase signalling controls microglia activation and neurotoxicity. *Nature* 472: 319–324.
64. Yang J-Y, Xue X, Tian H, Wang X-X, Dong Y-X, Wang F, *et al.* (2014): Role of microglia in ethanol-induced neurodegenerative disease: Pathological and behavioral dysfunction at different developmental stages. *Pharmacol Ther* 144: 321–337.
65. Marshall SA, McClain JA, Kelso ML, Hopkins DM, Pauly JR, Nixon K (2013): Microglial activation is not equivalent to neuroinflammation in alcohol-induced neurodegeneration: the importance of microglia phenotype. *Neurobiol Dis* 54: 239–251.
66. Qin L, Crews FT (2012): Chronic ethanol increases systemic TLR3 agonist-induced neuroinflammation and neurodegeneration. *J Neuroinflammation* 9: 130.
67. Marshall SA, Geil CR, Nixon K (2016): Prior Binge Ethanol Exposure Potentiates the Microglial Response in a Model of Alcohol-Induced Neurodegeneration. *Brain Sci* 6: E16.
68. Walter TJ, Crews FT (2017): Microglial depletion alters the brain neuroimmune response to acute binge ethanol withdrawal. *J Neuroinflammation* 14: 86.
69. Boretius S, Escher A, Dallenga T, Wrzos C, Tammer R, Brück W, *et al.* (2012): Assessment of lesion pathology in a new animal model of MS by multiparametric MRI and DTI. *NeuroImage* 59: 2678–2688.
70. Xie M, Tobin JE, Budde MD, Chen C-I, Trinkaus K, Cross AH, *et al.* (2010): Rostrocaudal analysis of corpus callosum demyelination and axon damage across disease stages refines diffusion tensor imaging correlations with pathological features. *J Neuropathol Exp Neurol* 69: 704–716.
71. Kong L, Lian G, Zheng W, Liu H, Zhang H, Chen R (2013): Effect of Alcohol on Diffuse Axonal Injury in Rat Brainstem: Diffusion Tensor Imaging and Aquaporin-4 Expression Study. *BioMed Res Int* 2013: 798261.
72. Wheeler-Kingshott CAM, Cercignani M (2009): About "axial" and "radial" diffusivities. *Magn Reson Med* 61: 1255–1260.
73. Acosta-Cabronero J, Williams GB, Pengas G, Nestor PJ (2010): Absolute diffusivities define the landscape of white matter degeneration in Alzheimer's disease. *Brain* 133: 529–539.
74. Mishra VR, Sreenivasan KR, Zhuang X, Yang Z, Cordes D, Walsh RR (2019): Influence of analytic techniques on comparing DTI-derived measurements in early stage Parkinson's disease. *Heliyon* 5: e01481.
75. Winklewski PJ, Sabisz A, Naumczyk P, Jodzio K, Szurowska E, Szarmach A (2018): Understanding the Physiopathology Behind Axial and Radial Diffusivity Changes—What Do We Know? *Front Neurol* 9. https://doi.org/10.3389/fneur.2018.00092
76. Aung WY, Mar S, Benzinger TL (2013): Diffusion tensor MRI as a biomarker in axonal and myelin damage. *Imaging Med* 5: 427–440.

77. Sun S-W, Neil JJ, Song S-K (2003): Relative indices of water diffusion anisotropy are equivalent in live and formalin-fixed mouse brains. *Magn Reson Med* 50: 743–748.
78. Sun S-W, Song S-K, Harms MP, Lin S-J, Holtzman DM, Merchant KM, Kotyk JJ (2005): Detection of age-dependent brain injury in a mouse model of brain amyloidosis associated with Alzheimer's disease using magnetic resonance diffusion tensor imaging. *Exp Neurol* 191: 77–85.
79. Wang Y, Wang Q, Haldar JP, Yeh F-C, Xie M, Sun P, *et al.* (2011): Quantification of increased cellularity during inflammatory demyelination. *Brain* 134: 3587–3598.
80. Kim JH, Wu T-H, Budde MD, Lee J-M, Song S-K (2011): Noninvasive detection of brainstem and spinal cord axonal degeneration in an amyotrophic lateral sclerosis mouse model. *NMR Biomed* 24: 163–169.
81. Kerbler GM, Hamlin AS, Pannek K, Kurniawan ND, Keller MD, Rose SE, Coulson EJ (2013): Diffusion-weighted magnetic resonance imaging detection of basal forebrain cholinergic degeneration in a mouse model. *NeuroImage* 66: 133–141.
82. Tournier J-D, Mori S, Leemans A (2011): Diffusion tensor imaging and beyond. *Magn Reson Med* 65: 1532–1556.
83. Badea A, Delpratt NA, Anderson RJ, Dibb R, Qi Y, Wei H, *et al.* (2019): Multivariate MR biomarkers better predict cognitive dysfunction in mouse models of Alzheimer's disease. *Magn Reson Imaging* 60: 52–67.
84. Qin W, Zhang M, Piao Y, Guo D, Zhu Z, Tian X, *et al.* (2012): Wallerian Degeneration in Central Nervous System: Dynamic Associations between Diffusion Indices and Their Underlying Pathology. *PLOS ONE* 7: e41441.
85. Santis SD, Cosa-Linan A, Garcia-Hernandez R, Dmytrenko L, Vargova L, Vorisek I, *et al.* (2020): Chronic alcohol consumption alters extracellular space geometry and transmitter diffusion in the brain. *Sci Adv* 6: eaba0154.
86. Somkuwar SS, Villalpando EG, Quach LW, Head BP, McKenna BS, Scadeng M, Mandyam CD (2021): Abstinence from ethanol dependence produces concomitant cortical gray matter abnormalities, microstructural deficits and cognitive dysfunction. *Eur Neuropsychopharmacol J Eur Coll Neuropsychopharmacol* 42: 22–34.
87. Mielenz D, Reichel M, Jia T, Quinlan EB, Stöckl T, Mettang M, *et al.* (2018): EFhd2/Swiprosin-1 is a common genetic determinator for sensation-seeking/low anxiety and alcohol addiction. *Mol Psychiatry* 23: 1303–1319.
88. Rando K, Hong K-I, Bhagwagar Z, Li C-SR, Bergquist K, Guarnaccia J, Sinha R (2011): Association of frontal and posterior cortical gray matter volume with time to alcohol relapse: a prospective study. *Am J Psychiatry* 168: 183–192.
89. Chumin EJ, Grecco GG, Dzemidzic M, Cheng H, Finn P, Sporns O, *et al.* (2019): Alterations in White Matter Microstructure and Connectivity in Young Adults with Alcohol Use Disorder. *Alcohol Clin Exp Res* 43: 1170–1179.
90. Bullmore E, Sporns O (2009): Complex brain networks: graph theoretical analysis of structural and functional systems. *Nat Rev Neurosci* 10: 186–198.
91. Melozzi F, Bergmann E, Harris JA, Kahn I, Jirsa V, Bernard C (2019): Individual structural features constrain the mouse functional connectome. *Proc Natl Acad Sci U S A* 201906694.
92. Kimbrough A, Lurie DJ, Collazo A, Kreifeldt M, Sidhu H, Macedo GC, *et al.* (2020): Brain-wide functional architecture remodeling by alcohol dependence and abstinence. *Proc Natl Acad Sci U S A* 117: 2149–2159.
93. Griffin WC, Ramachandra VS, Knackstedt LA, Becker HC (2015): Repeated cycles of chronic intermittent ethanol exposure increases basal glutamate in the nucleus accumbens of mice without affecting glutamate transport. *Front Pharmacol* 6: 27.
94. Lovinger DM, Alvarez VA (2017): Alcohol and basal ganglia circuitry: Animal models. *Neuropharmacology* 122: 46–55.
95. Whitfield-Gabrieli S, Thermenos HW, Milanovic S, Tsuang MT, Faraone SV, McCarley RW, *et al.* (2009): Hyperactivity and hyperconnectivity of the default network in schizophrenia and in first-degree relatives of persons with schizophrenia. *Proc Natl Acad Sci* 106: 1279–1284.

96. Hoffman RE, Fernandez T, Pittman B, Hampson M (2011): Elevated Functional Connectivity Along a Corticostriatal Loop and the Mechanism of Auditory/Verbal Hallucinations in Patients with Schizophrenia. *Biol Psychiatry* 69: 407–414.
97. Degiorgis L, Karatas M, Sourty M, Faivre E, Lamy J, Noblet V, *et al.* (2020): Brain network remodelling reflects tau-related pathology prior to memory deficits in Thy-Tau22 mice. *Brain J Neurol* 143: 3748–3762.
98. Fornito A, Zalesky A, Breakspear M (2015): The connectomics of brain disorders. *Nat Rev Neurosci* 16: 159–172.
99. Bosse KE, Ghoddoussi F, Eapen AT, Charlton JL, Susick LL, Desai K, *et al.* (2019): Calcium/calmodulin-stimulated adenylyl cyclases 1 and 8 regulate reward-related brain activity and ethanol consumption. *Brain Imaging Behav* 13: 396–407.
100. Juarez B, Morel C, Ku SM, Liu Y, Zhang H, Montgomery S, *et al.* (2017): Midbrain circuit regulation of individual alcohol drinking behaviors in mice. *Nat Commun* 8: 2220.
101. Liu Y, Montgomery SE, Juarez B, Morel C, Zhang S, Kong Y, *et al.* (2020): Different adaptations of dopamine release in Nucleus Accumbens shell and core of individual alcohol drinking groups of mice. *Neuropharmacology* 175: 108176.
102. Raichle ME (2015): The brain's default mode network. *Annu Rev Neurosci* 38: 433–447.
103. Jonckers E, Delgado y Palacios R, Shah D, Guglielmetti C, Verhoye M, Van der Linden A (2014): Different anesthesia regimes modulate the functional connectivity outcome in mice: Anesthesia and Functional Connectivity Outcome in Mice. *Magn Reson Med* 72: 1103–1112.
104. Grandjean J, Schroeter A, Batata I, Rudin M (2014): Optimization of anesthesia protocol for resting-state fMRI in mice based on differential effects of anesthetics on functional connectivity patterns. *NeuroImage* 102: 838–847.
105. Bukhari Q, Schroeter A, Cole DM, Rudin M (2017): Resting State fMRI in Mice Reveals Anesthesia Specific Signatures of Brain Functional Networks and Their Interactions. *Front Neural Circuits* 11: 5.
106. Grandjean J, Canella C, Anckaerts C, Ayrancı G, Bougacha S, Bienert T, *et al.* (2020): Common functional networks in the mouse brain revealed by multi-centre resting-state fMRI analysis. *NeuroImage* 205: 116278.
107. Riihioja P, Jaatinen P, Haapalinna A, Kiianmaa K, Hervonen A (1999): EFFECTS OF AGEING AND INTERMITTENT ETHANOL EXPOSURE ON RAT LOCUS COERULEUS AND ETHANOL-WITHDRAWAL SYMPTOMS. *Alcohol Alcohol* 34: 706–717.
108. Bordier C, Weil G, Bach P, Scuppa G, Nicolini C, Forcellini G, *et al.* (2022): Increased network centrality of the anterior insula in early abstinence from alcohol. *Addict Biol* 27: e13096.
109. Haaranen M, Scuppa G, Tambalo S, Järvi V, Bertozzi SM, Armirotti A, *et al.* (2020): Anterior insula stimulation suppresses appetitive behavior while inducing forebrain activation in alcohol-preferring rats. *Transl Psychiatry* 10: 150.
110. Jaramillo AA, Randall PA, Frisbee S, Besheer J (2016): Modulation of sensitivity to alcohol by cortical and thalamic brain regions. *Eur J Neurosci* 44: 2569–2580.
111. Gehrlach DA, Weiand C, Gaitanos TN, Cho E, Klein AS, Hennrich AA, *et al.* (2020): A whole-brain connectivity map of mouse insular cortex ((K. M. Wassum & Y. Livneh, editors)). *eLife* 9: e55585.
112. Namkung H, Kim S-H, Sawa A (2017): The Insula: An Underestimated Brain Area in Clinical Neuroscience, Psychiatry, and Neurology. *Trends Neurosci* 40: 200–207.
113. Campbell EJ, Flanagan JPM, Walker LC, Hill MKRI, Marchant NJ, Lawrence AJ (2019): Anterior Insular Cortex is Critical for the Propensity to Relapse Following Punishment-Imposed Abstinence of Alcohol Seeking. *J Neurosci* 39: 1077–1087.
114. Droutman V, Read SJ, Bechara A (2015): Revisiting the role of the insula in addiction. *Trends Cogn Sci* 19: 414–420.
115. De Oliveira Sergio T, Lei K, Kwok C, Ghotra S, Wegner SA, Walsh M, *et al.* (2021): The role of anterior insula–brainstem projections and alpha-1 noradrenergic receptors for

compulsion-like and alcohol-only drinking [no. 11]. *Neuropsychopharmacology* 46: 1918–1926.
116. Campbell EJ, Lawrence AJ (2021): It's more than just interoception: The insular cortex involvement in alcohol use disorder. *J Neurochem*. https://doi.org/10.1111/jnc.15310
117. Tabakoff B, Munoz-Marcus M, Fields JZ (1979): Chronic ethanol feeding produces an increase in muscarinic cholinergic receptors in mouse brain. *Life Sci* 25: 2173–2180.
118. Basser PJ, Pierpaoli C (1996): Microstructural and physiological features of tissues elucidated by quantitative-diffusion-tensor MRI. *J Magn Reson B* 111: 209–219.

LEGENDS TO FIGURES

Figure 1: Chronic alcohol exposure: experimental design and drinking behavior.

A. Experimental design of the two-bottle choice drinking alcohol paradigms, consisting in 20 sessions of 24h hours of access to alcohol (ALC mice, n=11) or water (CTRL mice, n=12) for 45 days. Alcohol consumption over time is represented in **B**. **C.** 24h after the last alcohol access session, mouse brain MRI is acquired combining resting-state functional MRI (rsfMRI), advanced-DTI and anatomical imaging sequences to respectively investigate functional connectivity, structural connectivity and morphological brain changes. Brains were then collected for immunohistology of microglia cells (IBA1 and GFAP).

Figure 2. Signatures of structural modifications upon voluntary alcohol drinking.

Multivariate data driven analysis was performed using several quantitative MR-based parameters reflecting structural tissue characteristics. Structural MRI parameters include axial diffusivity (AD), associated to longitudinal diffusivity of water molecules along tissues; radial diffusivity (RD) informing perpendicular diffusion to the longitudinal axis; mean diffusivity (MD) extracted from rotationally invariant diffusion in a voxel; fractional anisotropy (FA) corresponding to a normalized measure of diffusion direction (118); fiber density (FD) extracted using tractography algorithms to calculate the intervoxel connectivity, and morphological deformation (logjacobian). Voxels with significant inter-groups differences in the GM (**A**) and the WM (**E**) between ALC (n=11) and CTRL (n=12) groups (ALC vs. CTRL groups) are shown in red ($p<0.05$ uncorr; freedom degree = 21. **B, C, D.** Data driven clustering results identify three main clusters of inter-group differences (ALC vs. CTRL), with specific multivariate signatures presented in the associated radar plots. Dark blue circles represent CTRL group values; larger circles show an increase from CTRL values and smaller circles indicate a decrease. Significant differences between groups (ALC vs. CTRL) at $p<0.05$ ($z=2$) are represented by light blue circles, and at $p<0.01$ ($z = 3$) in red circles. **B.** Coronal slices show the first cluster covering prefrontal cortex (PFC) and partly rostral

agranular insular (AI) areas characterized by similar parametric signatures (associated plot shows higher AD, RD, MD, FA, FD and lower volume in ALC mice), **C.** The cluster covering dorsal hippocampal brain regions (dHIP) shows lower diffusivity (AD, RD, MD) and higher FA, FD and volume in ALC than CTRL group. **D.** The cluster covering somatosensory (SS) and motor areas is characterized by lower diffusivity (AD, RD, MD) and FD, higher FA and smaller volume in ALC than in CTRL group. **F.** A significantly different WM cluster was found covering the corpus callosum (cc) and the external capsule (ec) characterized by lower diffusivity (AD, RD, MD), higher FA and smaller volume in ALC than in CTRL group.

Figure 3. Microglia modifications upon voluntary alcohol drinking.

A. Representative images of IBA1 staining are shown in the PFC of CTRL and ALC mice, exemplifying counting (top panels) and thresholding approaches to segment on the IBA1 staining the morphology of the microglial cells (red) and to measure the % IBA1 stained area. **B.** Quantitative histopathological analysis of IBA1 staining in the prefrontal cortex (PFC), the insular cortex (AI), and the hippocampus (HIP) in CTRL (grey) and ALC (blue) mice Differences between groups were evaluated regarding the density of positive cells (cells/100000µm^2) and the stained % area (two-sample t-tests; *p<0.05; **p<0.01; ***p<0.001; ****p<0.0001).

C and **D**. Quantitative parameters derived from advanced-DTI and histological differences reaching statistical significance in inter-group comparison, and are represented in Z-score (*p<0.05, **p<0.01). The radar-plots in **C and D** show the pattern (dark blue line) of combined results including significant group differences in MD, RD, AD, FD, FA, IBA1 stained % area, IBA1 density of positive cells, and logjacobian in AI/PFC and HIP. The green lines indicate the p<0.05 thresholds of significance (increase or decrease) relative to the CTRL group parameters – bold grey line. Giving a global perspective on the pathological state of the PFC, **C** shows a potential relationship between the significant increase of all diffusivity-related quantitative MRI parameters and a microglial response reflecting an increased number of IBA1 cells but a decrease of %stained area in ALC mice due to

shrinkage of microglial processes. **D.** In HIP, the plot illustrates a different pathological pattern than in the PFC, showing a significant increase in FA only, associated with an increase of both the number and the coverage percentage of microglial cells in the HIP.

Figure 4. Remodeling of functional connectivity across 26 brain regions upon voluntary alcohol drinking.

A, B. Network diagrams for each group (**A** – CTRL group n=12; **B** – ALC group n=11) of the brain functional connectivity. Statistically significant connections ($p<0.01$, FDR corrected; CTRL freedom degree = 11; ALC freedom degree = 10) are presented as lines connecting the nodes in each graph (thickness is correlated with the connection strength, and colors with the correlation coefficient value). The size of nodes indicates the "hubness" property while their color reflects the "degree" property of the respective node (higher in green). Histograms represent the ranking of significantly connected nodes according to the degree, and the hubness coefficient of each node. **A.** In CTRL mice dorsal hippocampus (dHIP), DORpm thalamic nucleus (thalamus polymodal association cortex-related) and caudate putamen (CP) present the highest degree (rank 1, highest degree = 7). Cortical retrosplenial area (RSP) and pallidum (PAL) were ranked equally on the second position (degree = 6), followed by septal nuclei (SEP) (rank 3, degree = 5). Nodes of basal ganglia system showed particular prominence within the global FC matrix: the caudate putamen (CP), pallidum (PAL), septal nuclei (SEP) and bed nuclei of the stria terminalis (BST) were ranked 2nd, 3rd, 4th and 6th respectively (CP: degree = 7; hubness = 7.2; PAL: degree = 6; hubness = 7; SEP: degree = 5, hubness = 6.9; BST: degree = 4, hubness = 6.5). Reward-aversion related nodes such as the accumbens nucleus (ACB), ventral tegmental area (VTA), raphe nucleus (RAmb) or habenula (HBN) showed comparative degree values (degree = 4) but different influences in hubness. The RSP presented a high degree of connectivity and hubness (degree = 6; hubness = 5). The insular cortex (AI) showed strong significant connectivity particularly towards prefrontal cortex (PFC), VTA, piriform cortex and CP. **B.** In ALC mice, we found higher maxima and lower minima of significantly connected nodes, in both degree (ALC: max

= 8, min = 1; CTRL: max = 7, min = 2) and hubness (ALC: max = 10.3, min = 1.14; CTRL: max =7.7, min = 1.3), when compared to CTRL mice. The most significant node in degree was the dHIP, also showing higher hubness values in ALC group (9.6) then in CTRL (6.7) group. RSP was found as one of the most influential nodes in the ALC brains, showing the highest hubness values, and ranked 2nd for the number of significant connections (degree = 7; hubness = 10.3). The reward related nodes such as ACB, VTA and RAmb decreased their hubness (ACB: hubness = 3.3 in ALC group vs. 4.6 in CTRL group; VTA and RAmb: not significant hubness in ALC group). The aversion related nodes strengthened their importance as hubs, including the HBN (hubness = 5.7 in ALC group vs. 4.6 in CTRL group) and the central amygdala (CEA hubness = 1.1 in ALC vs. not significant in CTRL). **C and D** show inter-groups comparison graphs (ALC vs CTRL) of the brain functional connectivity. Statistically significant differences ($p<0.01$, FDR corrected) were calculated according to the Stouffer coefficient. **C.** Ranking of most different nodes between ALC and CTRL groups (Stouffer analysis, $p<0.05$, uncorr., freedom degree = 21) is provided in the histogram. Tables show all significantly different connections (edges) between groups (***$p<0.001$, **$p<0.01$, *$p<0.05$). Four separate sections are presented, to get together the AI changed connections, the DMN-related areas (RSP and ACA), and the VTA. The last section shows significantly modified edges between all other nodes. **D.** Differences between ALC and CTRL brain FC are graphically represented on a sagittal brain view, showing both significantly changed nodes (green circles) and significantly different edges (red lines, increased FC; blue lines, decreased FC). Connection strength differences are depicted on a scale of correlation coefficients.

[Abbreviations: anterior cingulate area (ACA); nucleus accumbens (ACB); agranular insular cortex (AI); auditory area (AUD); basolateral/basomedial amydgalar nuclei (BLA/BMA); bed nuclei of the stria terminalis (BST); caudate putamen (CP); central amygdalar nucleus (CEA); dorsal hippocampus (dHIP); thalamus polymodal association cortex related (DORpm); thalamus sensory-motor related (DORsm); habenula (HBN); primary motor cortex (MOp); periaqueductal grey (PAG); pallidum (PAL); piriform cortex (PIR); prefrontal cortex (PFC);

perirhinal/ectorhinal/entorhinal cortex (PERI/ECT/ENT or fHIP); Raphe nucleus (RAmb); retrosplenial cortex (RSP); septum nucleus (SEP); primary somatosensory cortex (SSp); temporal association area (TEa); ventral hippocampus (vHIP); visual area (VIS); ventral tegmental area (VTA)]

Figure 5. Remodeling of seed-voxelwise functional connectivity for most changed nodes upon voluntary alcohol drinking. Inter-group (ALC vs. CTRL) differences in the functional connectivity patterns derived from seed-based analysis for: **A.** agranular insula (AI); **B.** ventral tegmental area (VTA); **C.** retrosplenial cortex (RSP). Voxel-wise inter-groups statistical comparison was carried out on seed-based connectivity maps, using a two-sample t-test, $p<0.05$, FDR cluster corrected, freedom degree = 21. Scales represent t-values for contrasts: ALC FC > CTRL FC in red (there was no significant ALC FC < CTR). **D.** Summary scheme of functional seed-based analysis showing key FC modifications for each of the three selected seeds (AI, VTA and RSP) in addition to differences in prefrontal cortex (PFC – suppl. Figure 2A), amygdala (AMG - suppl. Figure 2B), bed nuclei of stria terminalis (BST– suppl. Figure 2C) and somatosensory cortex (SS - suppl. Figure 2D). Alcohol exposure strongly impacted the functional connectivity of all these centers with limbic areas, known to mediate reward/aversion and stress responses (accumbens - ACB; AMG; habenula – HBN; caudate putamen – CP and BST). Additionally, the network drivers displayed perturbed functional connectivity towards brain areas that shown structural MRI parametric modifications: PFC; Anterior cingulate area – ACA, SS and hippocampus – HIP. Red lines indicate increased connectivity in ALC group, while blue lines indicate weakened FC in alcohol drinking mice, compared to CTRL.

[Abbreviations: anterior cingulate area (ACA); nucleus accumbens (ACB); agranular insular cortex (AI); amygdala (AMG); caudate putamen (CP); habenula (HBN); hippocampus (HIP); motor cortex (MO); midbrain reticular nucleus (MRN); retrosplenial cortex (RSP); reuniens nucleus (Rn); substantia nigra (SN); somatosensory cortex (SS); thalamus (TH); ventral tegmental area (VTA)]

Figure 6. Summary of key structural and functional modifications in mice upon voluntary alcohol drinking.

Schematic representation of key structural and functional findings. Centers identified from open-ended multivariate structural analysis are shown (PFC/AI, SS, HIP, grey). Centers identified from graph theory results among 26 regions of interest (AI, green; VTA, red; RSP, yellow) are shown combined with seed-based FC mapping data, highlighting significantly altered cross-talk between salience network (AI connectivity - green), reward-aversion circuitry (VTA connectivity – red) and default mode network (RSP connectivity - orange) in the ALC group. Alcohol exposure strongly impacted FC of these centers with limbic areas, known to mediate reward/aversion and stress responses (acumbens – ACB; amygdala – AMG; habenula – HBN; caudate putamen – CP and bed nuclei of stria terminalis – BST). Additionally, these driver networks displayed perturbed FC towards brain areas that showed structural MRI parametric differences: prefrontal cortex – PFC; Anterior cingulate area – ACA, somatosensory cortex – SS and hippocampus – HIP. Solid lines indicate increased connectivity, while dashed lined indicate weakened FC in alcohol drinking mice, compared to CTRL.

[Abbreviations: anterior cingulate area (ACA); nucleus accumbens (ACB); agranular insular cortex (AI); amygdala (AMG); bed nucleus of stria terminals (BST); caudate putamen (CP); thalamus polymodal association cortex related (DORpm); thalamus sensory-motor related (DORsm); habenula (HBN); hippocampus (HIP); piriform cortex (PIR); prefrontal cortex (PFC); retrosplenial cortex (RSP); raphe nucleus (RAmb); reuniens nucleus (Rn); septal nuclei (SEP); somatosensory cortex (SS); ventral tegmental area (VTA)]

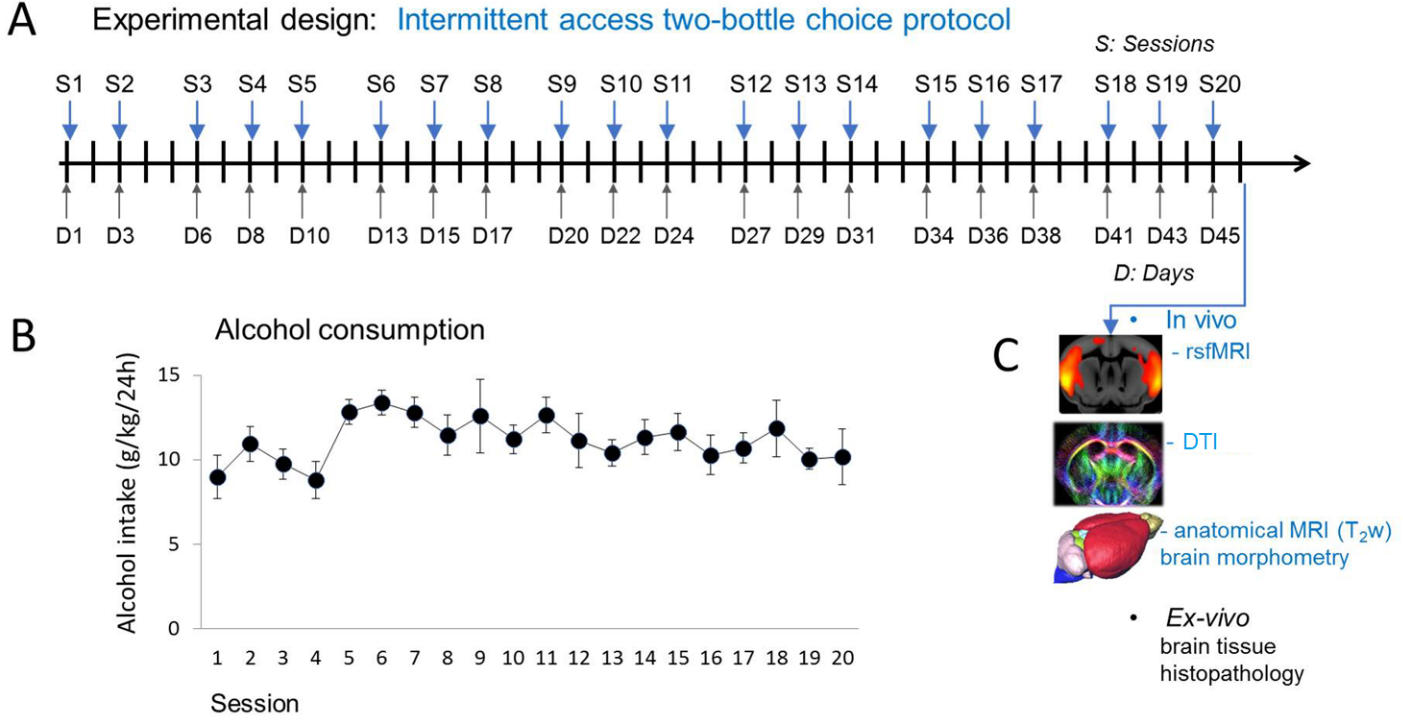
A
Experimental design: Intermittent access two-bottle choice protocol
S: Sessions
S1 S2 S3 S4 S5 S6 S7 S8 S9 S10 S11 S12 S13 S14 S15 S16 S17 S18 S19 S20
D1 D3 D6 D8 D10 D13 D15 D17 D20 D22 D24 D27 D29 D31 D34 D36 D38 D41 D43 D45
D: Days
B
Alcohol consumption
Alcohol intake (g/kg/24h)
15
10
5
0
1 2 3 4 5 6 7 8 9 10 11 12 13 14 15 16 17 18 19 20
Session
C
• In vivo
- rsfMRI
- DTI
- anatomical MRI (T_2w)
brain morphometry
• Ex-vivo
brain tissue
histopathology

A Mean significant gray matter cluster

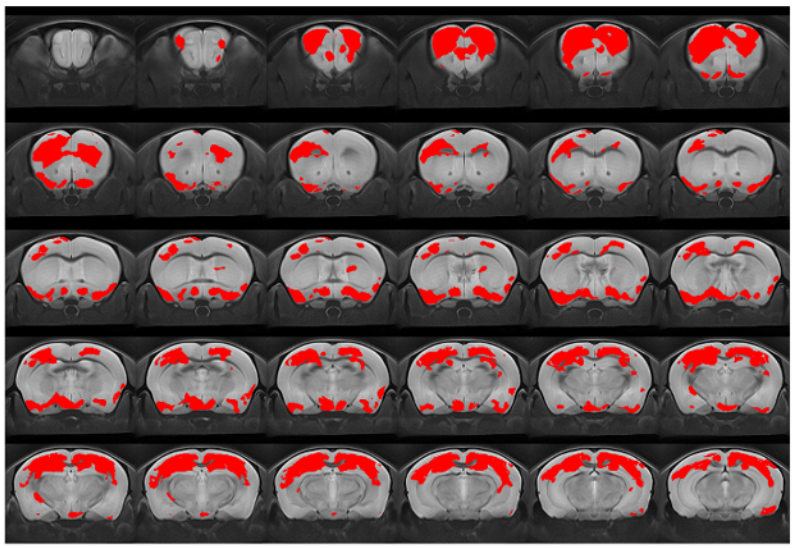

B PFC/AI cluster

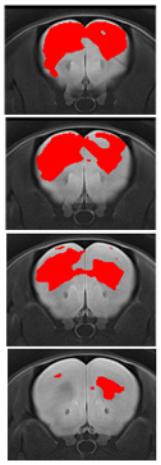

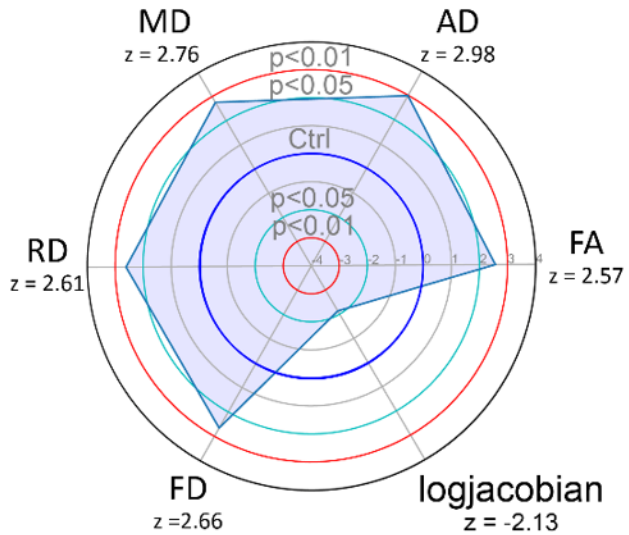

C dHIP cluster

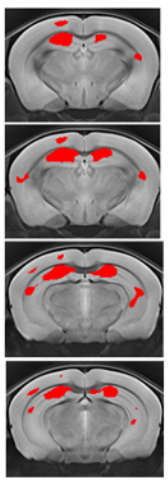

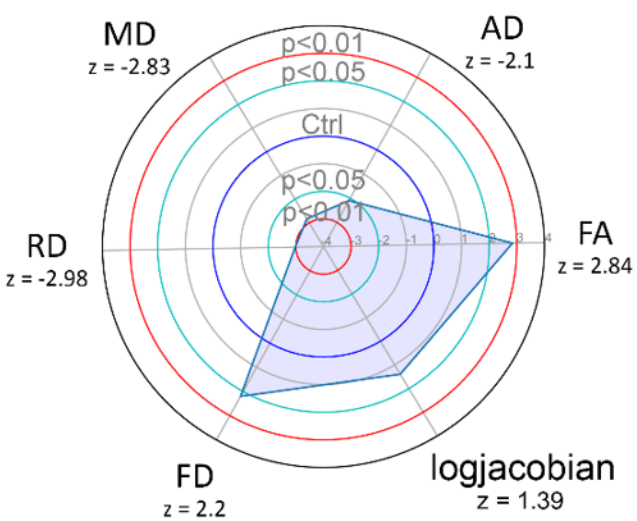

D SS cluster

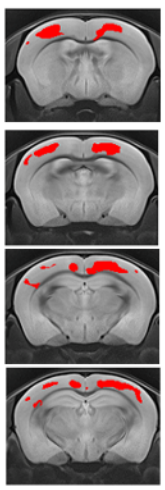

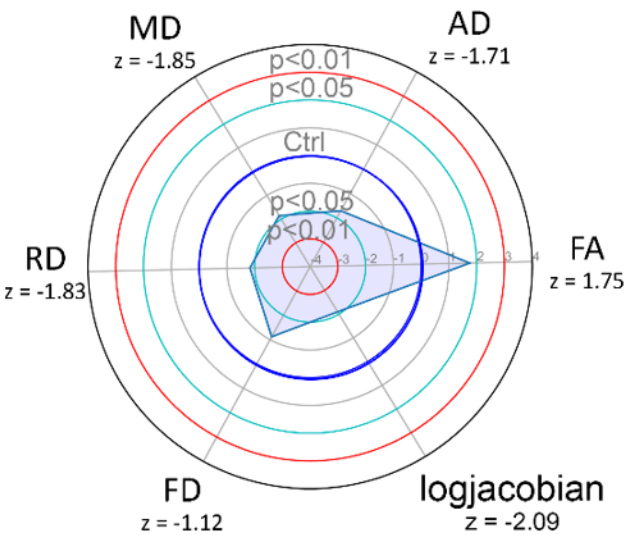

E Mean significant white matter cluster

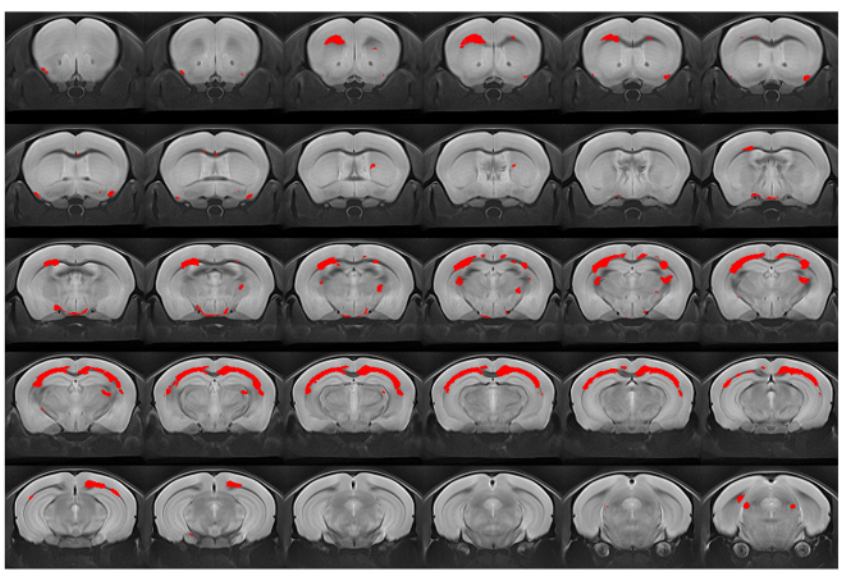

F Corpus callosum cluster

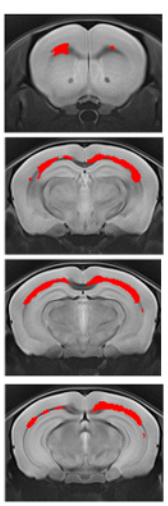

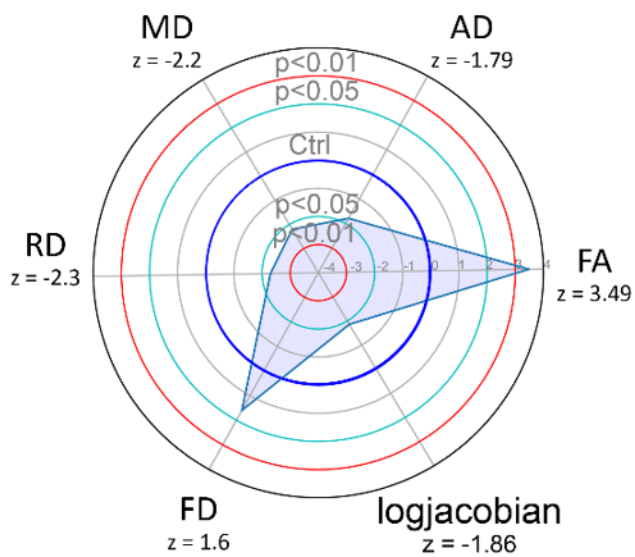

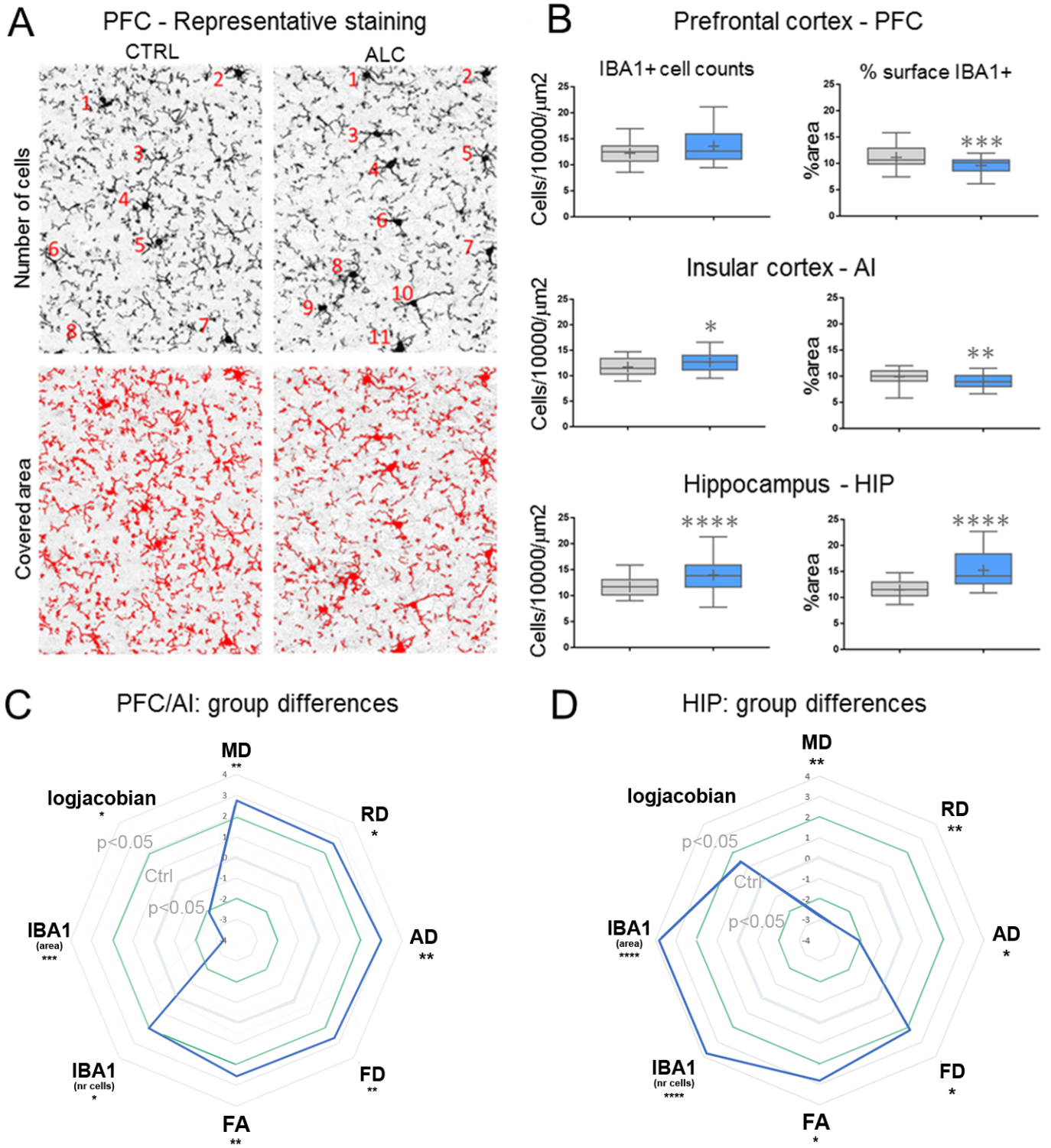
A
PFC - Representative staining
CTRL
ALC
Number of cells
Covered area
B
Prefrontal cortex - PFC
IBA1+ cell counts
% surface IBA1+
Cells/10000/µm2
%area
***
Insular cortex - AI
*
**
Hippocampus - HIP
****
****
C
PFC/AI: group differences
MD
**
RD
*
AD
**
FD
**
FA
**
IBA1
(nr cells)
*
IBA1
(area)
***
logjacobian
*
p<0.05
Ctrl
p<0.05
D
HIP: group differences
MD
**
RD
**
AD
*
FD
*
FA
*
IBA1
(nr cells)
****
IBA1
(area)
****
logjacobian
p<0.05
Ctrl
p<0.05

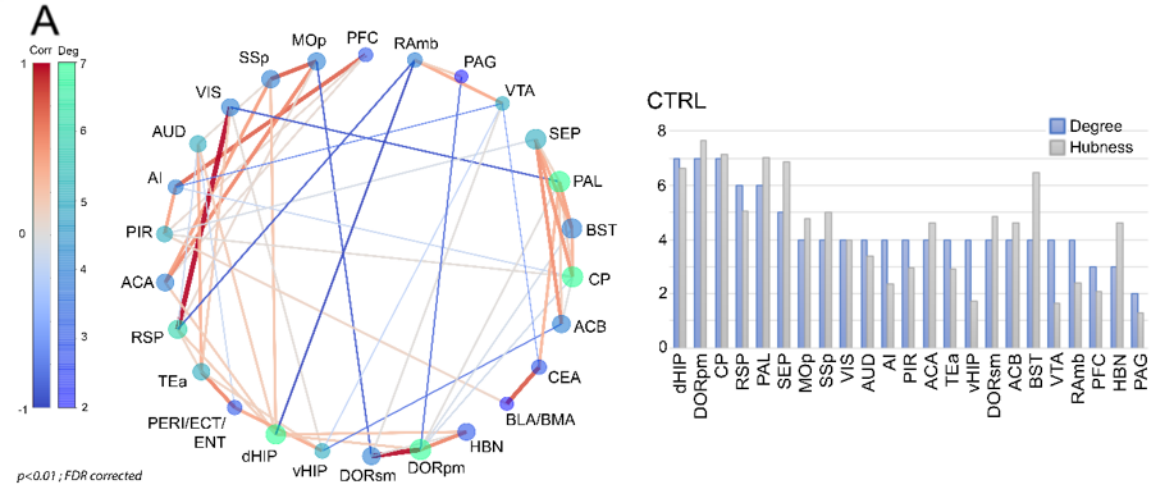

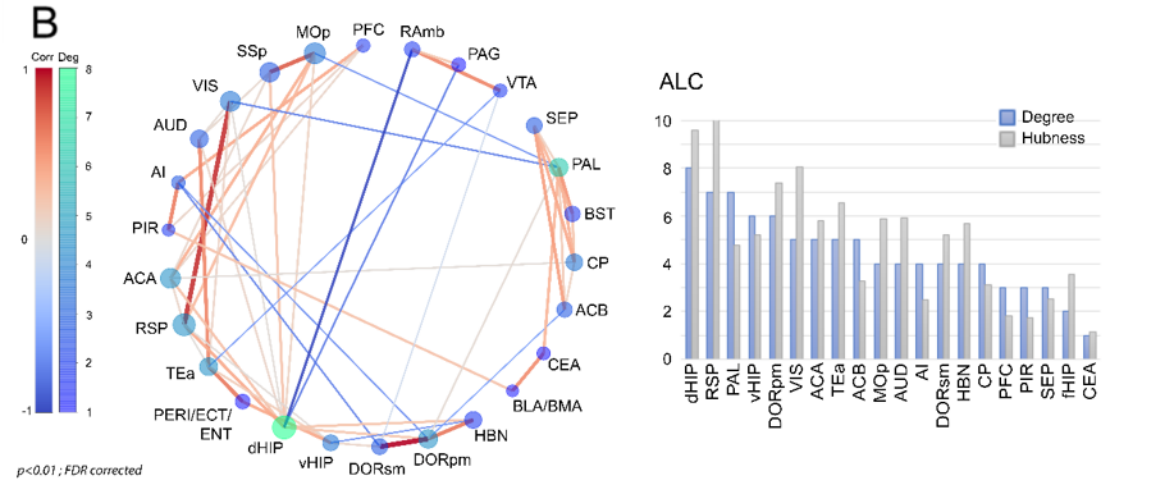

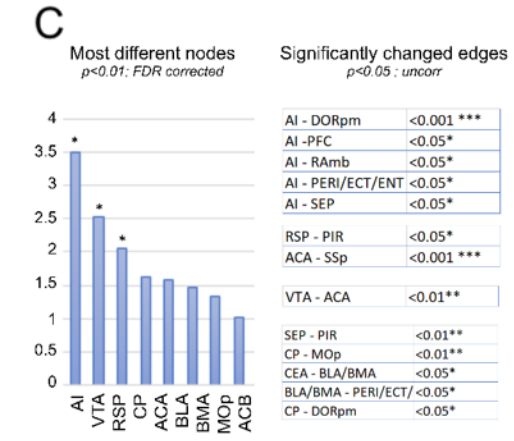

Significantly changed edges
p<0.05 ; uncorr

AI - DORpm	<0.001 ***
AI -PFC	<0.05*
AI - RAmb	<0.05*
AI - PERI/ECT/ENT	<0.05*
AI - SEP	<0.05*
RSP - PIR	<0.05*
ACA - SSp	<0.001 ***
VTA - ACA	<0.01**
SEP - PIR	<0.01**
CP - MOp	<0.01**
CEA - BLA/BMA	<0.05*
BLA/BMA - PERI/ECT/	<0.05*
CP - DORpm	<0.05*

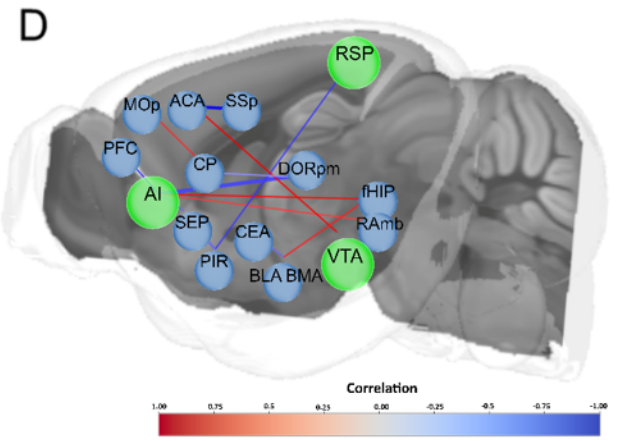

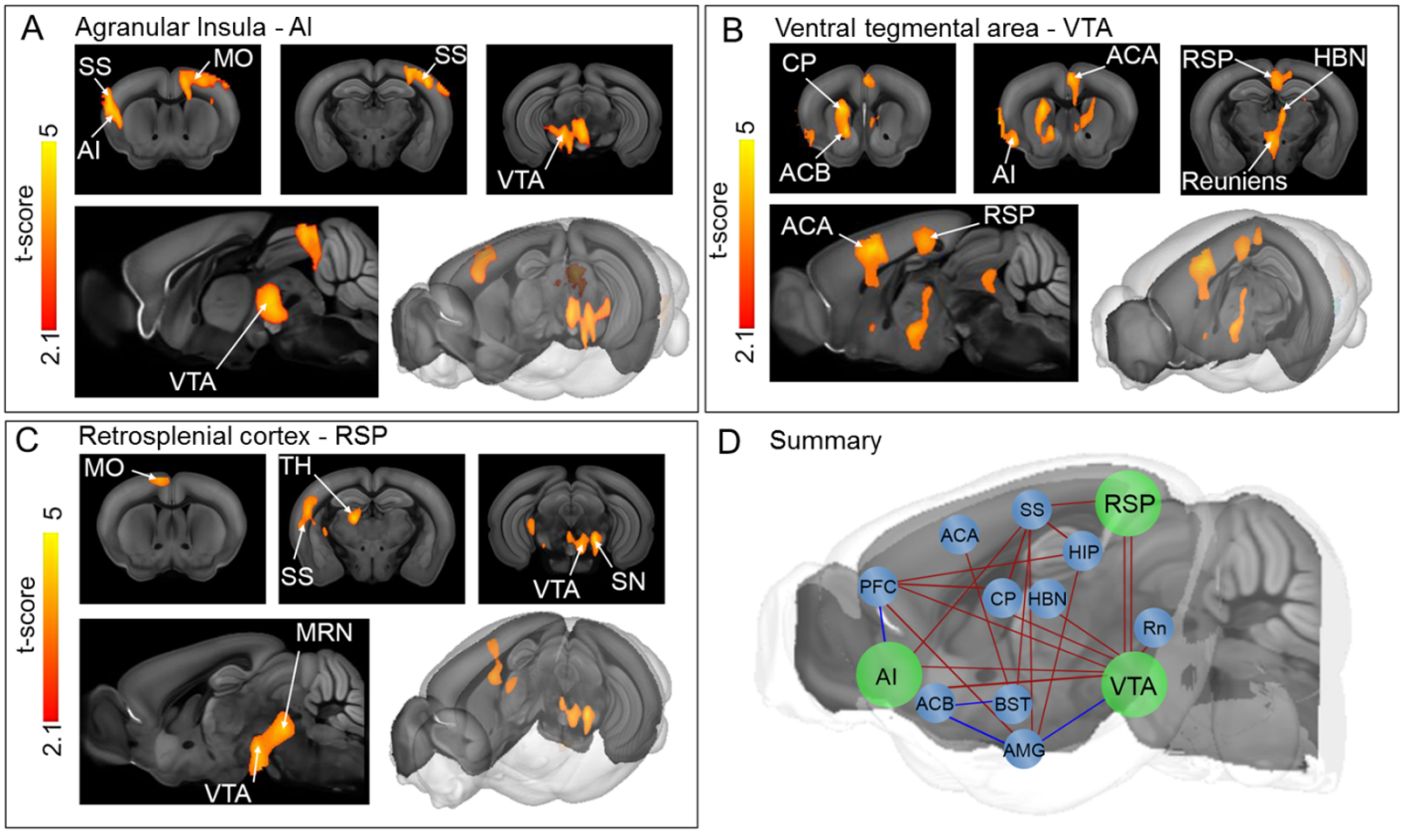
A
Agranular Insula - AI
SS
MO
AI
SS
VTA
t-score
5
2.1
VTA
B
Ventral tegmental area - VTA
CP
ACB
ACA
AI
RSP
HBN
Reuniens
t-score
5
2.1
ACA
RSP
C
Retrosplenial cortex - RSP
MO
TH
SS
VTA
SN
t-score
5
2.1
MRN
VTA
D
Summary
RSP
SS
ACA
HIP
PFC
CP
HBN
Rn
AI
VTA
ACB
BST
AMG

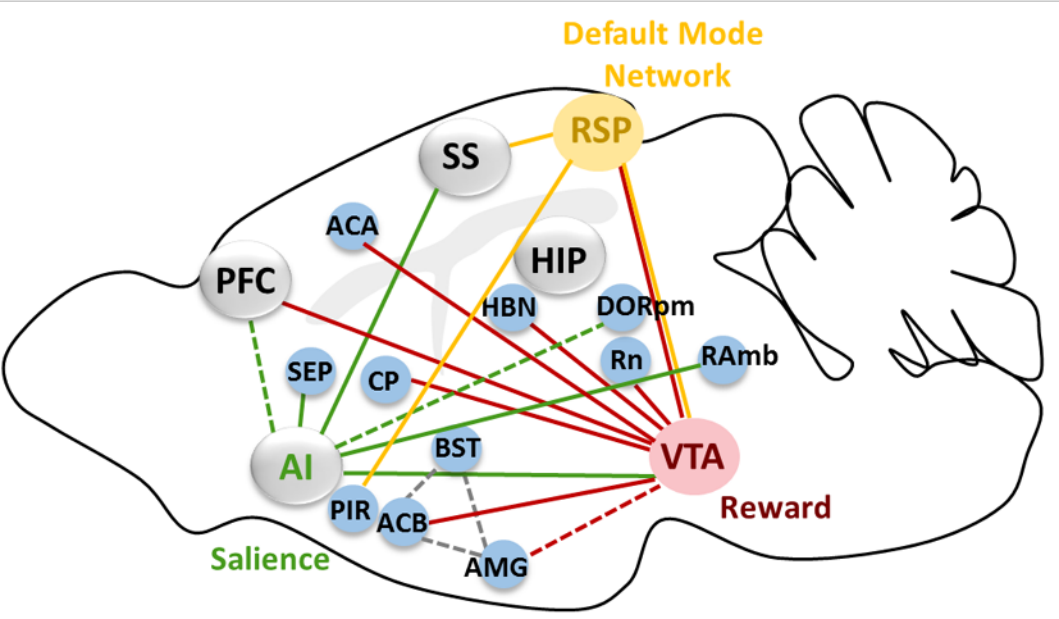
Default Mode
Network
RSP
SS
ACA
HIP
PFC
HBN
DORpm
Rn
RAmb
SEP
CP
AI
BST
VTA
PIR
ACB
Reward
Salience
AMG